release of SF_6 at a depth of 4000 m in the Brazil Basin of the South Atlantic. It revealed a very different regime, where mixing is 10 to 100 times as strong as at the lesser depths sampled by the 1992 to 1994 experiment (*8*). Indirect measurements spanning the basin were also performed that detected elevated mixing in the deepest ocean over jagged features such as mid-ocean ridges, but not over smooth abyssal plains (*9*). The findings sparked a flurry of studies that converged on a common conclusion: Tidal currents flowing over peaks and valleys launch undersea waves, which in turn power elevated mixing (*10*, *11*). This process largely governs the structure of the abyssal ocean and contributes substantially to the dissipation of tides.

The third major tracer-release experiment is described by Schmitt *et al.* (see the figure) (*2*). Performed in 2001, it targeted yet another distinct mixing regime which, though modest in extent, is exotic. In the upper tropical Atlantic, immediately east of the Caribbean, the ocean organizes itself into 10 or so steps, each 10 to 30 m high, which can be laterally coherent for hundreds of kilometers. Each step consists of a well-mixed layer bounded above and below by relatively thin interfaces in which temperature and salinity decrease sharply with depth.

This grand "thermohaline staircase" clearly owes its existence to salt fingers, which are centimeter-scale rising and sinking tendrils that develop where warmer and saltier water overlies cooler, fresher water. In laboratory and numerical experiments, salt fingers mix salinity much more effectively than they mix heat (*12*, *13*), but such a dichotomy had not been firmly established in the ocean. The difference in mixing rates arises (as does salt fingering itself) because molecular diffusion of salt is 100 times slower than the diffusion of heat; thus, excess salinity is "locked" into sinking fingers, whereas excess heat tends to leak away. Because SF_6 diffuses at nearly the same rate as salt, its transport by salt fingering should also be comparable.

Based on SF_6 dispersion, Schmitt *et al.* deduce a mixing rate for salinity that is approximately double that inferred indirectly for temperature. This rate is intermediate between the mixing rates in the upper eastern North Atlantic (*7*) and those in the deep Brazil Basin (*8*). A crucial property of mixing by salt fingering is that it tends to enhance the density contrasts between the abyssal and upper ocean, whereas mixing driven by tides and winds reduces the density contrasts.

The results reported by Schmitt *et al.* (*2*) supply one more piece of a puzzle that oceanographers must assemble to achieve a fuller understanding of ocean mixing. This understanding will in turn lead to more accurate and reliable models of the oceans and of climate.

References and Notes

1. Lateral stirring by ocean eddies, leading ultimately to mixing through pathways that are not well understood, also plays a role. Land-sea exchanges such as geothermal heating and river runoff are important in certain locations.
2. R. W. Schmitt, J. R. Ledwell, E. T. Montgomery, K. L. Polzin, J. M. Toole, *Science* **308**, 685 (2005).
3. S. M. Griffies *et al.*, *Ocean Model.* **2**, 123 (2000).
4. W. Munk, *Deep-Sea Res.* **13**, 707 (1966).
5. T. R. Osborn, C. Cox, *Geophys. Fluid Dyn.* **3**, 321 (1972).
6. T. R. Osborn, *J. Phys. Oceanogr.* **10**, 83 (1980).
7. J. R. Ledwell, A. J. Watson, C. S. Law, *J. Geophys. Res.* **103**, 21499 (1998).
8. J. R. Ledwell *et al.*, *Nature* **403**, 179 (2000)
9. K. L. Polzin, J. M. Toole, J. R. Ledwell, R. W. Schmitt, *Science* **276**, 93 (1997).
10. C. Garrett, *Science* **301**, 1858 (2003).
11. E. Kunze, S. G. Llewellyn Smith, *Oceanography* **17**, 55 (2004).
12. R. W. Schmitt, *Prog. Oceanogr.* **56**, 419 (2003).
13. J. Yoshida, H. Nagashima, *Prog. Oceanogr.* **56**, 435 (2003).

10.1126/science.1111417

STRUCTURAL BIOLOGY

Nature's Rotary Electromotors

Wolfgang Junge and Nathan Nelson

Molecular motors abound in the cell. Myosin motors power muscle contraction, kinesin motors move vesicles from one end of the cell to the other, and the ribosome processes along RNA. These linearly operating molecular motors are all powered by cleavage of the universal "fuel" molecule ATP (adenosine 5′-triphosphate). The ATP synthase (or F-ATPase), which produces ATP, is a fine example of one of nature's rotary motors. F-ATPase consists of two coupled motors, one electrically driven and the other chemically driven. There are several types of rotary motors, but only three are electrically driven: the F_0-portion of the F-type ATPase, the V_0-portion of V-type ATPases, and the flagellar motor of bacteria. The first two obey similar construction principles, whereas the bacterial flagellar motor is quite different. But all three types of rotary motor contain a central, ion-binding rotor ring that is embedded in the respective coupling membrane of the cell. The first high-resolution crystal structures of this ring are now revealed by Meier *et al.* on page 659 (*1*) and Murata *et al.* on page 654 (*2*) of this issue. Meier and colleagues report the structure at 0.24-nm resolution of the c ring of the F-type Na^+-ATPase from *Ilyobacter tartaricus* (*1*). Meanwhile, Murata and co-workers present the structure at 0.21-nm resolution of the K ring of the V-type Na^+-ATPase from the bacterium *Enterococcus hirae* (*2*). Some of the newly revealed properties are in keeping with current mechanistic models, whereas others defy previous postulates.

F-type ATPases usually synthesize ATP at the expense of ion-motive force, whereas V-type ATPases generate ion-motive force at the expense of ATP hydrolysis. Some ATPase subunits share sequence homology, whereas others are unique to each ATPase family (*3*). ATPases transport either protons (H^+) or less commonly sodium cations (Na^+) across their respective coupling membrane. These enzymes are constructed from two rotary motors—the ion-driven motor F_0 and the chemical generator F_1 in F-type ATPases, and the V_0 and V_1 motor/generators in V-type ATPases. The membrane-embedded F_0 and V_0 domains mediate the movement of either protons or Na^+ ions across the membrane, and the peripheral F_1 and V_1 domains interact with ADP, inorganic phosphate, and ATP (see the figure). F_0 and F_1, and V_0 and V_1, respectively, are mechanically coupled by a central rotating shaft and are held together by an eccentric stalk. The central shaft together with the ring to which it is firmly attached is termed the rotor, and the rest of the ATPase is called the stator. The ion-driven rotation of the central c ring in F-type ATPases or K ring in V-type ATPases relative to the peripheral subunits of the F_0 or V_0 domains generates torque. Transmission of this torque to the F_1 or V_1 domains drives them to operate over the three C_3-symmetrical reaction sites where ATP is assembled from or cleaved into ADP and inorganic phosphate in a stepped rotation. The c ring in F_0 is composed of 10, 11, or 14 identical polypeptides depending on the organism (*4*–*6*). The 10 to 14 steps that mark progression of the c ring are adapted to the nonmatching C_3 symmetry of F_1 owing to the elasticity of the rotary power transmission between the two motors, which is essential for their working together efficiently (*7*, *8*). Previous structural data for the c ring of F_0 were derived from nuclear magnetic resonance (NMR) (*9*), cryo–electron microscopy (cryo-EM) (*10*), x-ray crystallography (*6*), and atomic force microscopy (*4*, *5*). However, these structural data lacked sufficient resolution. An NMR

W. Junge is in the Division of Biophysics, University of Osnabrück, 49069 Osnabrück, Germany. E-mail: junge@uos.de N. N. Nelson is in the Department of Biochemistry, Tel Aviv University, 69978 Tel Aviv, Israel. E-mail: nelson@post.tau.ac.il

structure of the monomeric c subunit in a mixed solvent (*9*, *11*) has been widely used in modeling studies, and also for refining one x-ray–derived model of the c ring (*6*).

The new crystal structures of both the c ring of F_0 (*1*) and the K ring of V_0 (*2*) reveal a concave barrel with a pronounced waist in the middle, and an inner septum that is probably filled with and electrically sealed by membrane lipids in vivo. The K ring of V_0 is about twice as wide as the c ring of F_0, and Na^+ binding sites are found in the waist of both F_0 (*1*) and V_0 (*2*). Each protomer in the ring carries an essential, ion-binding glutamic acid residue (Glu) in the middle of the respective carboxyl-terminal helix: Glu^{65} in the hairpin-shaped subunit c of F_0 from *I. tartaricus* (*1*) and Glu^{139} in the subunit K double-hairpin of V_0 from *E. hirae* (*2*). To appreciate the new features of both structures, we need to consider how F_0 and V_0 may generate torque (*12*–*14*). The ring is thought to undergo Brownian rotational fluctuations relative to the membrane portion of the stator (see the figure). Fluctuations are subject to two electrostatic constraints: The essential glutamic acid residues in the ring must be negatively charged when facing the positive stator and neutralized by cation binding when facing hydrophobic membrane lipids (see the figure). Two access channels for ions—that are on either side of the stator, (and are not colinearly located), thus creating chirality—complete the electromotor. A cation that enters through the lower access channel and binds to the essential glutamic acid residue in the ring relieves the electrostatic constraint such that the ring is allowed to move one step farther counterclockwise. Thus, the cation concentration gradient determines the direction of rotary motion: counterclockwise if it is positive in the lower compartment, and clockwise if it is negative in the lower compartment. In this way, ion flow generates torque. This Brownian ratchet generates directed motion based on stochastic thermal fluctuations of the ring against the stator and of ions flowing into and out of the access channels. Since it was first proposed, this concept has been modified in two different ways: by invoking a swiveling motion of one of the two helices of the hairpin, and by assuming that the essential glutamic acid residue in the repetitive hairpins is directly accessible from one aqueous compartment. Both of these modifications are not supported by the new structures. First, the new c-ring crystal structure of F_0, unlike the previously assumed one, is now fully compatible with c-to-a cross-linking data (*15*, *16*). This eliminates the need to assume swiveling as pointed out by Meier and colleagues (*1*). Instead, the electromotor might operate by rotation of the rigid ring. Second, the one-channel model proposed by Dimroth's group (*13*, *17*) is not supported by the new ring structures, as Murata *et al.* point out (*2*). Neither the c-ring nor K-ring structures provide any obvious clues about the free accessibility from one side of the essential glutamic acid residue in the ring, but note the argument made by Meier *et al.* (*1*), who still favor free accessibility from one side.

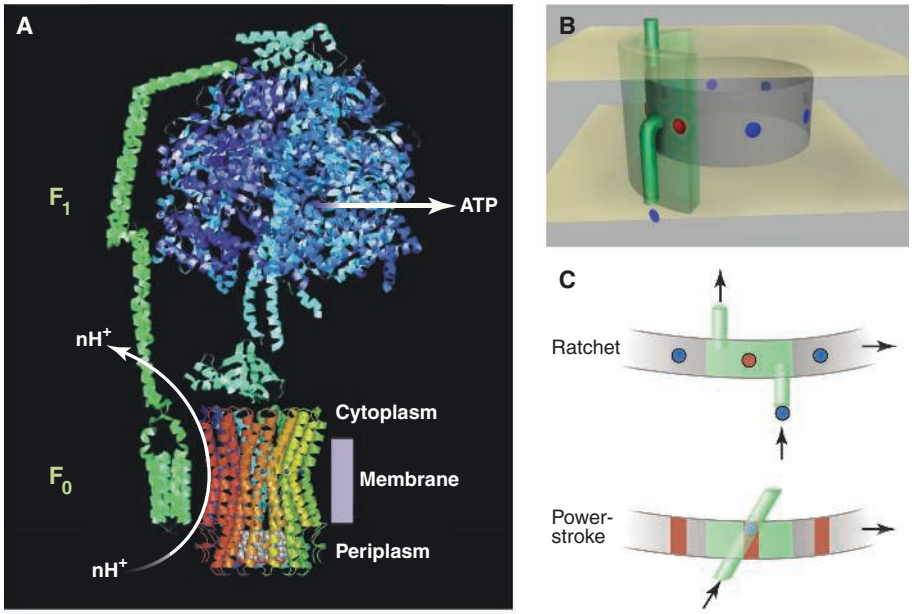

A turning point for ATPase. (**A**) The F-type ATPase is composed of the F_1 domain—which interacts with ATP, ADP, and phosphate—and the F_0 domain, which moves ions across the respective coupling membrane. Both domains are mechanically coupled by a central rotary shaft and an eccentric stalk. The membrane-embedded F_0 domain contains the c ring, formed from identical hairpin-shaped protomers. Ion flow (here proton flow) spins the c ring relative to peripheral subunits of F_0, thereby generating torque, which is transmitted by the rotary shaft to the F_1 domain. F_1 carries three reaction sites for ATP synthesis/hydrolysis. (The figure is composed of several partial structures of F-ATPase from various organisms.) (**B**) The Brownian rotary ratchet mechanism of ion conduction by an F-type ATPase (*12*, *21*). (**C**) Ratchet versus power-stroke mechanism of torque-generating ion translocation.

The two-channel-and-ring Brownian ratchet (*12*) remains a viable model for torque generation in both the F-type and V-type electromotors. An alternative is the power-stroke model (see the figure, C). In this model, a cation moves across the membrane only when positioned between two half-cylindrical channels at the point of their overlap, one half-channel being on the rotor and the other on the stator (*18*). Because of the oblique orientation of one half-channel and the straight orientation of the other, a moving cation forces the ring to rotate. This simple power-stroke-only mechanism (see the figure) is difficult to accept because the new ring structures show the bound ions moving around with the ring. The Brownian ratchet thus remains the most probable mechanism. Whether there are partial power-stroke elements at the interface of contact between the ring and the stator might be revealed by future high-resolution structures of the stator elements apposed to the ring.

It has come as a surprise to those working on V-type ATPases that the crystal structure of the Na^+-translocating K ring shows decameric symmetry (*2*). Indeed, Murata and co-workers recently proposed a heptameric structure on the basis of single-particle classification of cryo-EM images (*19*). On the one hand, this discrepancy will certainly prompt a reconsideration of the reliability of single-particle image analyses. On the other hand, it raises the question of whether the present K-ring structure of the V-type ATPase from *E. hirae* can be extrapolated to the V-type ATPases of other organisms.

The structural symmetry of the F_0 c ring (*10*–*14*) versus the c ring of F_1 implies a H^+-to-ATP stoichiometry of 3.3 to 4.7 (which favors ATP formation). In eukaryotic V-type ATPases, six (double hairpin-shaped) c subunits, each with only one ion-binding residue, may compose the c ring, equivalent to the K ring in *E. hirae*. This suggests an H^+- to-ATP stoichiometry of 2 to 1 (6 to 3), which would favor ATP hydrolysis and proton pumping against a large pH difference by the V-ATPase (*20*). This low gear ratio has been held responsible for the generation of a very acidic internal pH in certain organelles, for example, pH 2 in vacuoles of lemon fruit cells. This acidic pH, as well as a voltage of 250 mV generated by a V-type ATPase in the insect midgut, is difficult to reconcile with the presence of 10 K subunits forming the rotor ring of the V-type ATPases [gear ratio of 3.3 (10 to 3)]. The sug-

gestion by Murata *et al.* (*2*) that the same ratio may also be true for eukaryotic V-type ATPases implies that we may have to rethink how an internal pH of 2 is formed in the vacuoles of lemon cells or just accept that the c ring of eukaryotic V-type ATPases (assembled from three different gene products) has a different symmetry. High-resolution structures of the V_0 domain of the eukaryotic V-type ATPase will hopefully resolve this issue.

References and Notes

1. T. Meier, P. Polzer, K. Diederichs, W. Welte, P. Dimroth, *Science* **308**, 659 (2005).
2. T. Murata, I. Yamato, Y. Kakinuma, A. G. W. Leslie, J. E. Walker, *Science* **308**, 654 (2005); published online 31 March 2005 (10.1126/science.1110064).
3. N. Nelson, W. R. Harvey, *Physiol. Rev.* **79**, 361, (1999).
4. H. Stahlberg *et al.*, *EMBO Rep.* **2**, 229 (2001).
5. H. Seelert *et al.*, *Nature* **405**, 418 (2000).
6. D. Stock, A. G. Leslie, J. E. Walker, *Science* **286**, 1700 (1999).
7. W. Junge *et al.*, *FEBS Lett.* **504**, 152 (2001).
8. O. Pänke, D. A. Cherepanov, K. Gumbiowski, S. Engelbrecht, W. Junge, *Biophys. J.* **81**, 1220 (2001).
9. M. E. Girvin *et al.*, *Biochemistry* **37**, 8817 (1998).
10. J. Vonck *et al.*, *J. Mol. Biol.* **321**, 307 (2002).
11. V. K. Rastogi, M. E. Girvin, *Nature* **402**, 263 (1999).
12. W. Junge, H. Lill, S. Engelbrecht, *Trends Biochem. Sci.* **22**, 420 (1997).
13. P. Dimroth, H. Wang, M. Grabe, G. Oster, *Proc. Natl. Acad. Sci. USA* **96**, 4924 (1999).
14. W. Junge, *Photosynth. Res.* **80**, 197 (2004).
15. R. H. Fillingame, W. Jiang, O. Y. Dmitriev, P. C. Jones, *Biochim. Biophys. Acta* **1458**, 387 (2000).
16. R. H. Fillingame, O. Y. Dmitriev, *Biochim. Biophys. Acta* **1565**, 232 (2002).
17. P. Dimroth, U. Matthey, G. Kaim, *Biochim. Biophys. Acta* **1459**, 506 (2000).
18. P. Lauger, *Biophys. J.* **53**, 53 (1988).
19. T. Murata *et al.*, *J. Biol. Chem.* **278**, 21162 (2003).
20. H. Arai, G. Terres, S. Pink, M. Forgac, *J. Biol. Chem.* **263**, 8796 (1988).
21. For an animation see www.biologie.uni-osnabrueck.de/biophysik/junge.

10.1126/science.1112617

NEUROSCIENCE

Understanding Intentions: Through the Looking Glass

Kiyoshi Nakahara and Yasushi Miyashita

If you see a person sitting at a dining table and scooping out soup with a spoon, you naturally understand the person's intention is to eat the soup with the spoon. However, if a baby is sitting next to that person, the action of scooping out the soup may be followed by the action of feeding the baby. When we understand the intentions of other people through their actions, "action" (in this case, scooping out the soup) should be understood in context. What brain mechanisms link action understanding to a particular context? With regard to action understanding, a class of neurons in the brain called "mirror neurons" are thought to be important because of their amazing ability to transmit electrical impulses not only during the execution of a particular action, but also during observation of the equivalent action being carried out by someone else (*1*–*4*). The name mirror neuron reflects this remarkable degree of visuo-motor congruency. If mirror neurons also are involved in the understanding of intention, then they must be activated according to the context in which the action occurs. On page 662 of this issue, Fogassi *et al.* (*5*) explore mirror neurons in the inferior parietal cortex of the monkey brain, and report a relationship between mirror neurons and the encoding of the context under which actions occur. Their findings suggest that mirror neurons in the inferior parietal cortex may be responsible for understanding the intention of action in other people.

Mirror neurons were originally discovered in monkeys, first in the ventral premotor cortex of the frontal lobe and then in the inferior parietal cortex (*2*, *6*). Recordings from single neurons in the monkey brain revealed several interesting features of mirror neurons in addition to their congruent visuomotor responses (*2*). First, activation of mirror neurons appears to require biological motion; that is, even if a mirror neuron shows a specific response to the observation of grasping, it does not respond when grasping is achieved using an artificial tool such as pliers. Second, not only visual information but also the sound of a particular action (such as tearing paper) can induce mirror neurons to fire. Third, activation of mirror neurons requires the achievement of the goal of the action. For example, the observation of grasping an object can activate mirror neurons, but the observation of fake grasping in the absence of an object, or of the object but without any grasping action, cannot evoke such discharges. Interestingly, under conditions where monkeys clearly understand that the goal of action has been achieved, mirror neurons respond even when the end of the action is occluded from their sight.

The third property, the requirement of goal-directed action, prompts an expectation that, to some degree, mirror neurons participate in understanding the intention underlying action. However, because previous experiments identified this goal dependency only in terms of the contact between individuals and target objects, this property alone seems to be insufficient for understanding intentions that require information about the context or the "hypergoal" of actions. In their new work, Fogassi *et al.* (*5*) recorded the discharges of neurons in the rostral part of the inferior parietal cortex (areas PF and PFG) of the monkey brain as the monkeys carried out a behavioral test with different action contexts. These investigators identified neurons that not only have mirror properties but also are able to encode actions in a context-dependent way.

The authors introduced two action contexts (see the figure, B). Under one set of circumstances, monkeys reach toward and grasp a food pellet, then eat it; under the other set, monkeys reach toward and grasp a nonfood pellet and then place it inside a container. The action of grasping an object is a component common to the two situations, but one that is followed by two different final goals: grasp-to-eat or grasp-to-place. One population of neurons showed discharges specifically related to the grasping action. The activity of these grasping-related neurons was often modulated by the context of the action. For example, some of these neurons showed higher discharge rates during grasping followed by eating relative to grasping followed by placing, and some showed the opposite behavior. Control experiments supported the idea that this modulation was specifically dependent on the circumstance of the action, and was not due to differences in the target object (food or nonfood) or to kinematics (the path or velocity of motion.) These findings suggest that neurons in the inferior parietal cortex encode particular actions in context-dependent ways.

Of even more interest, the authors reveal that this context-dependent encoding of action has a close relationship with the mirror properties of neurons in areas PF and PFG (see the figure, C). They examined mirror neurons that fire during both grasping execution and grasping observation. Among these, some mirror neurons also exhibited context-dependent modulation, and selectivity of this modulation was preserved across both execution of the action and observation of the action carried out by another individual. Thus, if a mirror neuron exhibited higher firing rates during execution of a grasp-to-eat action relative to a grasp-to-place action, this neuron also exhibited greater activation dur-

The authors are in the Department of Physiology, University of Tokyo School of Medicine, Bunkyo-ku, Tokyo 113-0033, Japan. E-mail: nakahara@m.u-tokyo.ac.jp; yasushi_miyashita@m.u-tokyo.ac.jp